Impact of conductivity on Lorentzian and Fano resonant high-Q THz metamaterials: Superconductor, metal and perfect electric conductor

Srivastava, Yogesh Kumar; Singh, Ranjan

2017

Srivastava, Y. K., & Singh, R. (2017). Impact of conductivity on Lorentzian and Fano resonant high- Q THz metamaterials: Superconductor, metal and perfect electric conductor. Journal of Applied Physics, 122(18), 183104-.

https://hdl.handle.net/10356/86626

https://doi.org/10.1063/1.4994951

Impact of conductivity on Lorentzian and Fano resonant high-*Q* THz metamaterials: Superconductor, metal and perfect electric conductor

Yogesh Kumar Srivastava[1,2] and Ranjan Singh[1,2,a)]
[1]*Division of Physics and Applied Physics, School of Physical and Mathematical Sciences, Nanyang Technological University, Singapore 637371, Singapore*
[2]*Centre for Disruptive Photonic Technologies, The Photonics Institute, Nanyang Technological University, 50 Nanyang Avenue, Singapore 639798, Singapore*

(Received 9 July 2017; accepted 18 October 2017; published online 10 November 2017)

High temperature superconductors have created exciting opportunities for switchable metamaterial and plasmonic devices operating at terahertz frequencies. In recent times, there have been several demonstrations using superconducting metamaterials, such as thermal, electrical, magnetic, and optical switching. Here, we explore the impact of conductivity on terahertz metamaterial resonators with different resonance line shapes. Lorentzian and Fano line shaped resonators show different levels of enhancement in the quality factor and resonance intensity for metallic, superconductor, and perfect electric conductors, due to the interplay between the radiative and the non-radiative loss mechanisms in a metamaterial array. *Published by AIP Publishing.*
https://doi.org/10.1063/1.4994951

INTRODUCTION

With the advent of metamaterials,[1–5] there has been a tremendous advancement in the manipulation of the terahertz (THz) wave. This has led to the possibility of realizing various potential THz applications such as fingerprint chemical sensing, biosensing, modulators, non-linear THz devices for wireless communication channels, and many more.[6–10] Most of these applications demand for high quality factor (Q) resonance, either for enhanced localization of incident THz fields for high sensitivity sensors or higher spectral resolution in spectroscopy. The Q factor of the resonances in subwavelength metamaterial resonators is limited by the losses incurred in these structures due to the material and geometrical parameters. The two predominant loss mechanisms in metamaterials are – radiative loss and non-radiative loss. Radiative loss arises due to the radiative nature of the subwavelength resonator structures, whereas the non-radiative loss is primarily Ohmic that is due to the finite resistivity of the constituent material of the fabricated resonators. Tailoring of the material and structural parameters of the meta-atom for loss engineering has become an important aspect of metamaterial design to achieve high-Q values of resonances in real world devices.[11–19] The total quality factor (Q_T) of the metamaterial in terms of radiative and Ohmic losses is given by

$$\frac{1}{Q_T} = \frac{1}{Q_R} + \frac{1}{Q_O}, \tag{1}$$

where Q_R and Q_O represent the quality factor due to the radiative and Ohmic part, respectively.[17]

Hence, it is important to study the interplay between the radiative and the Ohmic losses in the resonator system to probe maximum achievable quality factors. In order to probe this interplay of losses in the metamaterial system, we chose two resonator designs – Lorentzian and Fano resonators, whose resonance properties are dominated by different loss mechanisms. The resonance line shape of the Lorentzian resonators is majorly determined by the large radiative loss, whereas the Fano resonance line shape is driven by the Ohmic loss of the resonator array. For the radiative loss driven metamaterial system, a single gap split ring resonator (SRR), which has Lorentzian (LC) line shaped resonance was chosen.[20,21] The LC resonance is a magnetic resonance that couples strongly with the free space, and results in higher radiative loss. This significantly hinders the enhancement of the Q factor in LC resonators.[49] We also chose a double gap asymmetric split ring resonator which supports a sharp asymmetric line shaped Fano resonance,[13,22,23] which is excited due to the interference between a broad continuum and a narrow discrete mode.[11–13,24–27] The Q factor and intensity of the Fano resonance are strongly dependent on the asymmetry of the structure.[28] In fact, the Q factor was shown to decline exponentially with increasing asymmetry of the structure.[29] Hence, in the low asymmetry regime of the Fano resonators, high-Q resonances are achieved whereas the high asymmetry regime results in Fano resonances with larger amplitude and broader linewidth. This is majorly due to the fact that as asymmetry decreases, the radiative loss is significantly suppressed and the overall loss in the system is dominated by the non-radiative Ohmic losses. Therefore, the conductivity of the materials for these resonators becomes critical in determining the maximum achievable Q factor. It is important to note that the SRR designs with extremely small gaps can also provide significantly high Q factors, however fabricating such samples with small gaps over a large area will require state-of-art fabrication facilities. Alternatively, Fano resonators provide practical advantage of allowing the access to sub-radiant high Q resonances at much larger gap dimensions ($\sim 3\,\mu$m), that can be fabricated using the conventional photolithography process.

a)ranjans@ntu.edu.sg

In order to maximize the Q factor of a given resonator, the best constituent material could be a hypothetical perfect electrical conductor (PEC), so that the Ohmic losses completely disappear. At THz frequencies, normal metals are highly conductive. However, with an extremely high Q resonance in a low asymmetry, the Fano resonator does not exist due to finite Ohmic loss in the system.[28] In the real world, extremely low-loss superconductors with drastically low Ohmic loss (at microwave and terahertz frequencies) could enable higher Q factor resonances compared to normal metals. Low-loss superconducting metamaterials at THz frequencies has been reported in literature. However, the performance of the resonance features in terms of high-Q factors is comparable to Drude metals in most of the cases.[30–33,37]

In this work, we have comprehensively analyzed the impact of a high temperature (high-T_c) superconductor YBCO in supporting low loss resonances at the THz spectral region in two different types of metamaterials, i.e., Lorentzian and Fano resonant metamaterials. We studied the influence of asymmetry in both Lorentzian and Fano resonances in terms of achievable Q factors and figure of merit (FoM). The FoM is defined as the product of the resonance quality factor and the intensity. Following this, we compared the performance of the superconductor resonators with that of metals and PEC in both resonator systems. The Drude metal based metamaterials at THz frequencies are limited by radiative and Ohmic losses, while PEC is an idealized hypothetical medium with infinite conductivity and so is purely limited by the radiative loss in the metamaterial array. Superconductors are realistic materials that have superior performance than Drude metals at THz frequencies. Through our investigations here, we observe that in the highly radiative regime, all the three material systems, i.e., the PEC, superconductor, and metal show nearly identical response in spite of a large difference in conductivity. However, in the Fano resonators with low structural asymmetry, where the radiative losses are low, the resonance response differs drastically. Highest Q factor and FoM are observed in the PEC system, followed by the superconductor and metal, respectively. Hence, the use of high-Tc superconductors over metals provides a good platform for achieving ultrahigh Q resonances in THz metamaterials. Superconductors also enable active control of coherence of superconducting Cooper-pairs using various external stimuli and have led to the demonstration of actively tunable superconducting meta-devices using temperature,[30–32] magnetic field,[33,34] electrical current,[35,36]and optical excitation.[37] The superconducting meta-devices have also shown interesting properties such as giant nonlinearity and macroscopic quantum effects, that could pave way for advanced THz meta-devices.[38–40]

DISCUSSION

Figures 1(a) and 1(b) show the schematic diagram of an array and unit cell of single gap SRR (MM1), respectively, which gives rise to the super-radiant Lorentzian LC resonance when the THz beam strikes the metamaterial sample at normal incidence with the electric field polarized parallel to the gap of the resonator (x-axis). Figures 1(c) and 1(d) show the schematic diagram of a double gap asymmetric split ring resonator (MM2) array and unit cell, respectively, which supports a sub-radiant Fano resonance when excited with an electric field polarized perpendicular to the gap of the resonator (y-axis). Asymmetry (d) in both of these resonators is defined as the displacement of a split gap of the resonator from the central vertical axis, as shown in Figs. 1(b) and 1(d). The value of d in the structures varies from 1 to 10 μm. The geometrical dimensions of MM1 are chosen to be smaller than those of MM2 to ensure that the LC and Fano resonances occur at the same frequency. For electromagnetic simulations, a commercially available software (CST microwave studio) is used. Sapphire, a THz transparent material with a dielectric constant of 11.7 and a thickness of 500 μm, is chosen as the substrate. Aluminum (Al) metal with a DC conductivity of 3.56×10^7 S/m is used to simulate the metallic structures. Since the electrical conductivity of the ultrathin metallic films does not change by more than two to threefold upon cooling to liquid nitrogen temperatures, the response of the metallic metamaterial at room temperature is used as a valid comparison with the superconductor metamaterial at low temperatures (see supplementary material).[41,42] The experimentally measured conductivity of the YBCO thin film [as shown in the inset of Fig. 2(b)] is used to define the dispersion of YBCO in simulation. The conductivity of the YBCO thin film was calculated from the THz amplitude and phase measurement at 27 K, which is much below the superconducting phase transition temperature of YBCO (~86 K).[43] As an ideal case, simulations were performed with PEC as the resonator material. Since, the conductivity of PEC is infinite, the losses in PEC resonator systems are purely governed by radiative mechanisms.

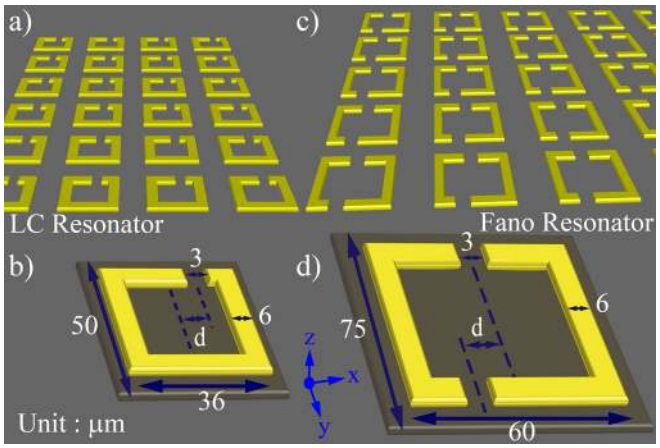

FIG. 1. Schematic diagram of the metamaterial: (a) and (b) represent the array and unit cell with geometrical dimensions of a single gap LC resonator (MM1). (c) and (d) represent the array and unit cell with geometrical dimensions of the double gap Fano resonators (MM2). "d" is the asymmetry, which is the displacement of the split gap from the central vertical axis.

The numerically calculated amplitude transmission spectra of MM1 with varying $d = 0$, 2, 5, and 10 μm are shown in Figs. 2(a)–2(d), respectively. For each of these d values, three material systems – the PEC (blue), superconductor (red), and metal (black) are simulated as shown in Fig. 2, respectively. The resonance amplitude transmission

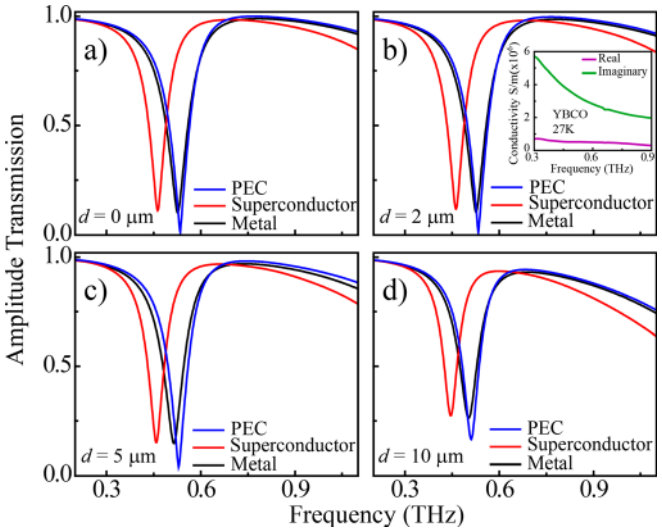

FIG. 2. Amplitude transmission spectra obtained from Lorentzian MM1 for the incident electric field polarized parallel to the gap arm of the structure: (a)–(d) represent the simulated transmission spectra with asymmetry $d = 0$, 2, 5, and 10 μm in MM1, respectively. The colour of the curves represents the PEC (blue), superconductor (red), and metal (black) materials used to design MM1. The inset in (b) represents the measured conductivity of the YBCO thin film at 27 K.

of PEC MM1, at lower asymmetries of $d = 0$ and 2 μm, is almost unity, and gradually decreases at higher asymmetry values of 5 and 10 μm. Metallic and superconducting MM1 structures result in almost similar response in terms of resonance strength and follow a similar trend as PEC for varying asymmetries of MM1. It is also important to note that the kinetic inductance of Cooper pairs in superconductors causes the red shift of the resonance in the superconducting resonator with the identical geometrical dimensions as a normal metal or PEC.[44] The lower resonance strength in metallic and superconducting resonators, compared to PEC is due to the presence of finite losses in real material systems. The superconducting resonances are slightly sharper as compared to the metallic counterpart because of its lower Ohmic loss. Since the superconductor and metal both result in a nearly identical response of LC resonant metamaterial, we conclude that as long as the material conductivity is high enough to support the super-radiant resonance, the geometrical parameter will play a dominant role in determining the resonance amplitude and linewidth. It must be stressed that superconductors possess frequency dependent conductivity which decreases as the frequency of operation increases beyond the microwaves.[45] From the two fluid model, the real (σ_{re}) and imaginary (σ_{im}) part of the complex conductivity of the superconductor are expressed as

$$\sigma_{re} = \frac{n_n e^2 \tau_n}{m^*(1+\omega^2 {\tau_n}^2)} \quad and \quad \sigma_{im} = \frac{n_s e^2}{m^* \omega} + \frac{n_n e^2 (\omega \tau_n)^2}{m^* \omega (1+\omega^2 {\tau_n}^2)}, \tag{2}$$

where n_n and n_s are the number densities of the normal particles and Cooper pairs, respectively, and the summation of the two is always a constant, i.e., $n_n + n_s = n$. The term τ_n represents the relaxation time of the normal particle, e is the electronic charge, m^* is the effective mass of the normal particles, and ω is the angular frequency of the incident radiation.[45,46] The above expression reflects that normal electrons contribute to Ohmic loss at non-zero frequencies which increases drastically beyond the microwave frequencies.

To better understand the impact of conductivity on the resonance response of metamaterials, we extend our studies to the sub-radiant Fano resonant metamaterials (MM2). The transmission spectra of MM2 with varying d value = 0, 2, 5, and 10 μm are shown in Figs. 3(a)–3(d), respectively. For each of the d values, the three material systems, i.e., the PEC (blue), superconductor (red), and metal (black), were simulated as shown in Fig. 3. The Fano resonance is a dark mode resonance since it is absent in the symmetric split ring resonators as shown in Fig. 3(a) and could only be excited by breaking the structural symmetry. As the asymmetry in the MM2 structure is introduced ($d = 2$ μm), we observe a well evolved sharp resonance at 0.5 THz in the PEC, whereas the superconductor and metal show weak Fano resonances as shown in Fig. 3(b). This observation clearly establishes the conductivity dependence of sub-radiant mode resonances. The sub-radiant Fano resonances have a larger lifetime (higher Q factor) and can sustain the local field for a longer period, while the field of the super-radiant mode decays in a shorter lifetime. The narrow linewidth and higher lifetime make the Fano resonances extremely sensitive to the Ohmic loss. As shown in Figs. 3(c) and 3(d), Fano resonances in the lossless PEC structures are stronger in comparison to metallic and superconducting resonators even at a larger asymmetry of $d = 5$ and 10 μm and the transmission amplitude at resonance approaches unity for PEC at $d = 10$ μm. However, for superconductors, the resonance linewidth is slightly sharper than the normal metal at all values of d, owing to the lower losses in superconductors compared to the metals. With the gradual increase in the asymmetry in the MM2, the resonance response of the metal and superconductor becomes comparable. The contrasting behavior of MM2 in

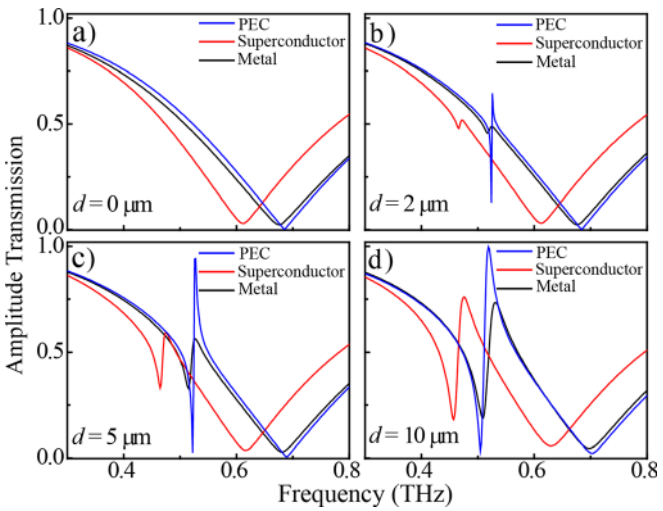

FIG. 3. Amplitude transmission spectra obtained from Fano MM2 for the incident electric field polarized perpendicular to the gap arm of the structure: (a)–(d) represent the simulated transmission spectra obtained from MM2 designed with the PEC, superconductor, and metal with asymmetry $d = 0$, 2, 5, and 10 μm, respectively.

low and high asymmetry regimes is due to the difference in the dominance of radiative losses at these asymmetries. At higher asymmetries ($d = 5$ and $10\,\mu$m), the coupling of the MM2 with free space increases which results in larger radiative loss. However, at lower asymmetries ($d = 2\,\mu$m), the radiative losses are largely suppressed due to weak coupling of MM2 to free space and even a small increase in conductivity of the constituent material results in a significant enhancement in the Q factor of resonances.

To experimentally validate the results, MM2 resonator arrays with an asymmetry of $d = 15\,\mu$m were fabricated with a YBCO superconductor and Al metal. A larger asymmetry sample that would have a broad resonance linewidth was chosen for the ease of measurement since our experimental set up has a measurement resolution of ~76 GHz. The superconductor metamaterial samples, with geometrical dimensions obtained from the simulation, were fabricated using the conventional photolithography technique on a commercially available 200 nm thick YBCO film deposited over a 500 μm thick r-cut sapphire substrate. The typical phase transition temperature and critical current density of this film are 85.1 K and 2.3 MA/cm^2, respectively. The identical metallic sample was fabricated using the lift-off process after photolithography, where 200 nm thick aluminum was deposited using the thermal evaporation method. Optical images of the metallic and superconducting samples are shown in Figs. 4(a) and 4(b), respectively. Transmission spectra of metamaterial samples were obtained by the ZnTe based THz spectroscopy setup.[47] The superconducting sample was cooled down to 27 K by using a continuous flow liquid helium cryostat, whereas the metallic sample was characterized at room temperature. The THz beam with a spot size of ~3 mm strikes the metamaterial sample (size 10 mm × 10 mm) at normal incidence with the E-field linearly polarized along the non-gap arms of the terahertz asymmetric split ring resonator. The transmission amplitude was estimated by the ratio of the transmitted electric field through the sample and reference and is given by $|\tilde{T}(\omega)| = |\tilde{E}_S(\omega)/\tilde{E}_R(\omega)|$, where $\tilde{E}_S(\omega)$ and $\tilde{E}_R(\omega)$ are the Fourier transform of the electric field transmitted through the sample and reference time domain pulse, respectively. Figures 4(c) and 4(d) depict the simulated and measured amplitude transmission spectra of superconducting (red curve) and metallic (black curve) samples, respectively. The difference in the linewidth of Fano resonances in the superconductor and metallic samples is about 9.85 GHz [Fig. 4(d)], which is consistent with the simulation results of 8.62 GHz as the difference in the linewidths shown in Figures 4(c). The experimentally measured Q factors for the superconducting and metallic samples are 5.89 and 5.22, respectively, which match well with the simulated Q factors of 6.03 and 5.86. Here, we use a slightly higher asymmetry ($d = 15\,\mu$m) sample instead of low asymmetry due to the limited measurement temporal resolution of 13.2 ps. The measured scan length is limited by Fabry–Perot reflections from the rear side of the sapphire substrate.

The linewidth of the resonance has a direct impact on the field confinement in the capacitive gap of the resonators. To better understand the contrasting behavior of MM1 and MM2, we plot the simulated electric field distribution at the

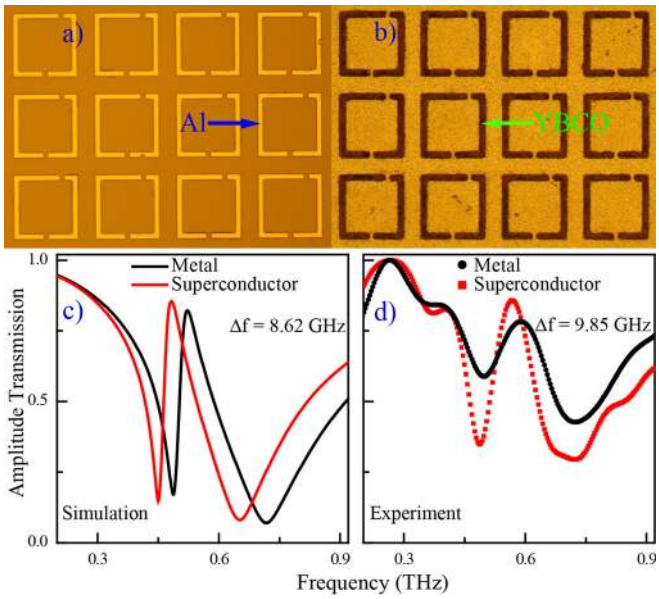

FIG. 4. (a) and (b) depict the optical image of the fabricated Fano resonator sample with aluminum and YBCO, respectively. (c) and (d) depict the simulated and measured amplitude transmission spectra, respectively, of the superconducting and metallic Fano resonators with asymmetry, $d = 15\,\mu$m. Δf is the difference in the linewidth of the superconducting and metallic sample.

resonance frequency for the asymmetry $d = 1\,\mu$m. Figures 5(a), 5(c), and 5(e) depict the electric field distribution of super-radiant MM1 at resonance frequencies for the PEC, superconductor, and normal metal cases, respectively. It is noted that all three materials show a tight field confinement in the capacitive gap of the MM1, and hence they result in almost a similar resonance response. Figures 5(b), 5(d), and 5(f) represent the electric field distribution of sub-radiant MM2 at resonance frequencies for the PEC, superconductor, and metal cases, respectively. In the case of PEC MM2 resonators, very high field confinement is observed in the capacitive gap, which confirms the excitation of a highly sub-radiant Fano resonance at low asymmetries. Superconducting MM2 shows stronger field confinement than the metallic counterpart and hence validates the origin of sharper resonances in the superconducting structures compared to metallic structures.

We further analyzed the Q factor of resonances in both the resonator systems (MM1 and MM2) to gain more physical insights. The Q factor of the Lorentzian resonance in MM1 is defined as the ratio of the resonance frequency (f_0) to the full width at half maxima (Δf) of the intensity, $Q = f_0/\Delta f$. Figure 6(a) shows the Q factors of MM1 for all three material systems, and it is clearly seen that the Q factors are nearly the same. However, the metallic MM1 structure shows slightly lower Q factors in comparison to the superconductor and PEC MM1 structures due to finite Ohmic losses. We note that the Q factors for PEC MM1 are slightly lower than the superconductors due to higher radiative loss in PEC (highest conductivity material) structures at a specific asymmetry. It must be noted that the onset of the dominant radiative loss regime for the highest conductivity asymmetric Fano resonators occur at the lowest asymmetry. Therefore, metamaterial asymmetric resonators of different

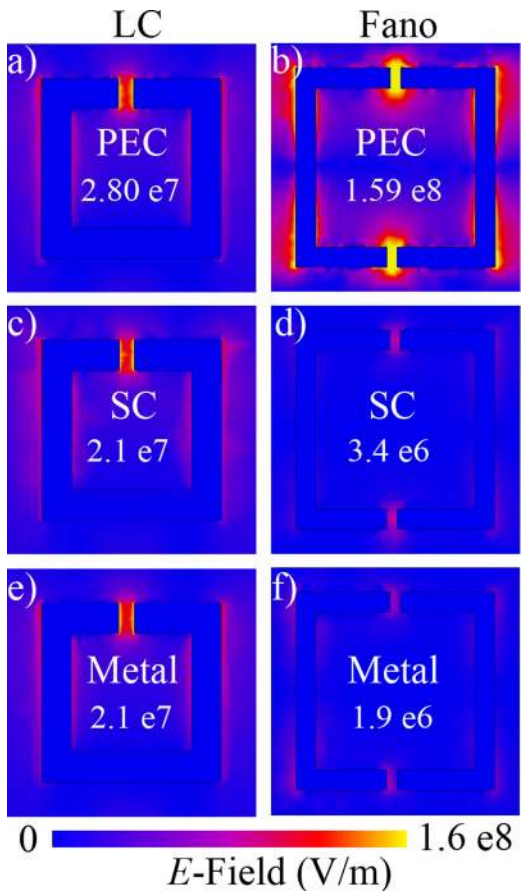

FIG. 5. Electric field distribution in LC and Fano resonators: (a), (c), and (e) represent the electric field distribution in MM1 at asymmetry $d = 1\,\mu$m designed with the PEC, superconductor, and metal, respectively. (b), (d), and (f) represents the electric field distribution in MM2 at asymmetry $d = 1\,\mu$m designed with the PEC, superconductor, and metal, respectively.

conductivities become highly radiative at different levels of structural asymmetry.

The Q factor of the MM2 resonators is calculated by fitting the transmitted intensity curve with the Fano parametric equation given by $T_{Fano} = |(a_1 + ja_2 + \frac{b}{\omega-\omega_0+j\gamma})|^2$, where a_1, a_2 and b are real constants, ω_0 is the Fano resonance frequency, and γ is the damping rate.[48] The Q factor was obtained as $Q = \frac{\omega_0}{2\gamma}$. Figure 6(b) shows the Q factors of MM2 for PEC, superconducting, and metallic resonators for varying asymmetries. From Figure 6(b), it can be noticed that the PEC structures result in a very high Q factor especially at a low asymmetry. For an asymmetry of $d = 0.3\,\mu$m, only PEC structures show resonances with a Q factor of 328, whereas metallic and superconducting resonators do not show any resonance. As the asymmetry increases to 1 μm, superconducting MM2 shows a sharp resonance with a Q factor of 167, whereas metallic MM2 shows resonances only above an asymmetry of $d = 1.8\,\mu$m. Superconductors enable access to the low asymmetry regime of MM2 which is otherwise inaccessible with normal metals. It is important to note that resonance excitation at lower asymmetries is key for achieving high-Q factor resonances as the Q factors of such symmetry broken structures decline exponentially with increasing asymmetry of the structures.[29] At lower asymmetries of up to $d = 3\,\mu$m, superconducting MM2 shows higher Q factor resonances in comparison to the metal. Superconductor and metallic MM2 result in similar Q factors at a higher asymmetry of $d > 5\,\mu$m. The difference in Q factors between PEC with superconductors and normal metals reduces drastically at higher asymmetries, which reflects weaker dependence of resonance properties on the conductivity of the resonator material as the metamaterial array transitions from a sub-radiant to a super-radiant regime. Highest Q factors observed using the

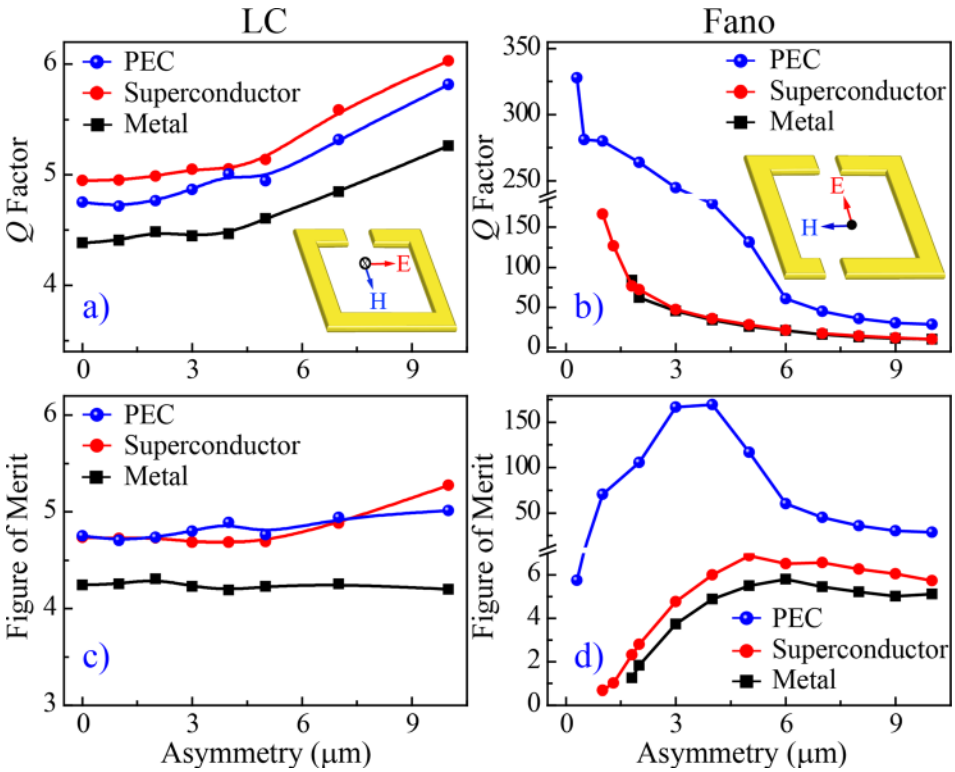

FIG. 6. Q Factor and FoM of LC (MM1) and Fano (MM2) resonances for the PEC, superconductor, and metal at varying asymmetries. (a) and (b) represent the Q Factor and (c) and (d) represent the figure of merit (FoM) obtained from MM1 and MM2 at different asymmetries, respectively.

PEC, superconductor, and metal are 328, 167, and 86, respectively.

We also studied the figure of merit (FoM) to describe the resonance response as the product of Q factor and the resonance transmission intensity (ΔI). The transmission intensity is estimated by the difference between the dip and peak of the resonance. The FoMs of PEC and superconducting MM1 structures are nearly identical (FoM$\sim$4.5–5.5) for all asymmetries, due to their low loss nature. Metallic MM1 structures result in a slightly lower FoM of $\sim$4.25 in comparison to superconductor but the difference is negligible. FoM values of MM2 are depicted in Figure 6(d) and it can be clearly seen that the FoM for PEC MM2 is more than an order of magnitude higher than the superconducting and metallic MM2. Superconducting MM2 results in significantly higher FoM values in comparison to the metallic counterpart at all asymmetries. Overall, we observe that the intrinsic conductivity of materials plays a dominant role in determining the resonance properties in MM2 (Fano resonance), whereas it is less important in MM1 (Lorentzian resonance).

The highest Q factor, narrower linewidth, and largest FoM are obtained for PEC Fano (MM2) structures and they depict the limit of highest attainable performance parameters in these resonator systems. However PEC is a hypothetical material, but serves as a design guide for high Q resonator systems. The high-T_c superconductors are realistic material systems, which are better suited to approach the maximum attainable limit of high-Q factors compared to metals in sub-radiant Fano systems. Hence, the combination of structural design of resonators and the material choice determines the overall resonance linewidth of a metamaterial array. Combined with the inherent advantage of low loss and natural response to various external stimuli, the superconductors are a promising candidate for interesting THz meta-device functionalities.

CONCLUSION

In summary, we have comprehensively studied the influence of asymmetry in structural design and conductivity of material systems in two different metamaterials, namely super-radiant Lorentzian and sub-radiant Fano resonant systems. We show that high conductivity materials, e.g., the PEC, superconductor, and metal have an almost identical resonance response in LC resonators, due to higher radiative losses which suppress the effect of small changes in the conductivity of the material on the resonance properties. However, in the case of asymmetric Fano line-shaped resonators with a low structural asymmetry, the conductivity strongly affects the Q factor and the resonance intensity of the Fano metamaterials. At a larger structural asymmetry, the Q factors of the resonances are identical for the superconductor and metal as the metamaterial transitions into the highly radiative regime. Superconductors are also suitable for supporting extremely sharp resonances in Fano resonators at the low asymmetry regime, which is inaccessible with high conductivity Drude metals. Superconducting Fano resonances enable significantly higher Q factor and FoM. Our results show that, along with the structural design engineering, the choice of material is vital for obtaining desired resonance response and affirms the superiority of superconductors in exciting narrow linewidth tunable resonances at THz frequencies.

SUPPLEMENTARY MATERIAL

See supplementary material for more details on the effect of material conductivity and cryogenic temperature on the Q factors of Fano resonators.

ACKNOWLEDGMENTS

The authors acknowledge the research funding support from the Singapore National Research Foundation (NRF) and the French National Research Agency (ANR), proposal No. NRF2016-NRF-ANR004.

[1]V. G. Veselago, Sov. Phys. Uspekhi **10**, 509 (1968).
[2]J. B. Pendry, A. Holden, D. Robbins, and W. Stewart, IEEE Trans. Microwave Theory Tech. **47**, 2075 (1999).
[3]D. R. Smith, W. J. Padilla, D. C. Vier, S. C. Nemat-Nasser, and S. Schultz, Phys. Rev. Lett. **84**(18), 4184 (2000).
[4]R. A. Shelby, D. R. Smith, and S. Schultz, Science **292**, 77 (2001).
[5]V. M. Shalaev, Nat. Photonics **1**, 41 (2007).
[6]W. Xu, L. Xie, and Y. Ying, Nanoscale **9**, 13864 (2017).
[7]M. Gupta, Y. K. Srivastava, M. Manjappa, and R. Singh, Appl. Phys. Lett. **110**, 121108 (2017).
[8]M. Manjappa, Y. K. Srivastava, A. Solanki, A. Kumar, T. C. Sum, and R. Singh, Adv. Mater. **29**, 1605881 (2017).
[9]H. Tao, L. R. Chieffo, M. A. Brenckle, S. M. Siebert, M. Liu, A. C. Strikwerda, K. Fan, D. L. Kaplan, X. Zhang, R. D. Averitt, and F. G. Omenetto, Adv. Mater. **23**, 3197 (2011).
[10]M. Kroner, A. O. Govorov, S. Remi, B. Biedermann, S. Seidl, A. Badolato, P. M. Petroff, W. Zhang, R. Barbour, B. D. Gerardot, R. J. Warburton, and K. Karrai, Nature **451**, 311 (2008).
[11]V. A. Fedotov, M. Rose, S. L. Prosvirnin, N. Papasimakis, and N. I. Zheludev, Phys. Rev. Lett. **99**, 147401 (2007).
[12]B. Luk'yanchuk, N. I. Zheludev, S. A. Maier, N. J. Halas, P. Nordlander, H. Giessen, and C. T. Chong, Nat. Mater. **9**, 707 (2010).
[13]W. Cao, R. Singh, I. A. I. Al-Naib, M. He, A. J. Taylor, and W. Zhang, Opt. Lett. **37**, 3366 (2012).
[14]S. M. Anlage, J. Opt. **13**(2), 024001 (2011).
[15]C. Kurter, P. Tassin, L. Zhang, T. Koschny, A. P. Zhuravel, A. V. Ustinov, S. M. Anlage, and C. M. Soukoulis, Phys. Rev. Lett. **107**, 043901 (2011).
[16]O. Limaj, F. Giorgianni, A. D. Gaspare, V. Giliberti, G. d. Marzi, P. Roy, M. Ortolani, X. Xi, D. Cunnane, and S. Lupi, ACS Photonics **1**, 570 (2014).
[17]G. Scalari, C. Maiseen, S. Cibella, R. Leoni, and J. Faist, Appl. Phys. Lett. **105**, 261104 (2014).
[18]I. Al-Naib, Y. Yang, M. M. Dignam, W. Zhang, and R. Singh, Appl. Phys. Lett. **106**(1), 011102 (2015).
[19]Y. K. Srivastava, M. Manjappa, L. Cong, W. Cao, I. Al-Naib, W. Zhang, and R. Singh, Adv. Opt. Mater. **4**, 457 (2016).
[20]R. Marques, F. Mesa, J. Martel, and F. Median, IEEE Trans. Antennas Propag. **51**, 2572 (2003).
[21]R. Singh, I. Al-Naib, M. Koch, and W. Zhang, Opt. Express **18**, 13044 (2010).
[22]U. Fano, Phys. Rev. **124**, 1866 (1961).
[23]A. E. Miroshnichenko, S. Flach, and Y. S. Kivshar, Rev. Mod. Phys. **82**, 2257 (2010).
[24]S. H. Mousavi, I. Kholmanov, K. B. Alici, D. Purtseladze, N. Arju, K. Tatar, D. Y. Fozdar, J. W. Suk, Y. Hao, A. B. Khanikaev, R. S. Ruoff, and G. Shvets, Nano Lett. **13**, 1111 (2013).
[25]R. Singh, I. A. I. Al-Naib, M. Koch, and W. Zhang, Opt. Express **19**, 6312 (2011).
[26]F. Miyamaru, S. Kubota, T. Nakanishi, S. Kawashima, N. Sato, M. Kitano, and M. W. Takeda, Appl. Phys. Lett. **101**, 051112 (2012).
[27]K. Aydin, I. M. Pryce, and H. A. Atwater, Opt. Express **18**, 13407 (2010).

[28]Y. K. Srivastava, M. Manjappa, H. N. S. Krishnamoorthy, and R. Singh, Adv. Opt. Mater. **4**, 1875 (2016).
[29]L. Cong, M. Manjappa, N. Xu, I. Al-Naib, W. Zhang, and R. Singh, Adv. Opt. Mater **3**, 1537 (2015).
[30]J. Gu, R. Singh, Z. Tian, W. Cao, Q. Xing, M. He, J. W. Zhang, J. Han, H.-T. Chen, and W. Zhang, Appl. Phys. Lett. **97**, 071102 (2010).
[31]H.-T. Chen, H. Yang, R. Singh, J. F. O'Hara, A. K. Azad, S. A. Trugman, Q. X. Jia, and A. J. Taylor, Phys. Rev. Lett. **105**, 247402 (2010).
[32]V. A. Fedotov, A. Tsiatmas, J. H. Shi, R. Buckingham, P. de Groot, Y. Chen, S. Wang, and N. I. Zheludev, Opt. Express **18**, 9015 (2010).
[33]B. Jin, C. Zhang, S. Engelbrecht, A. Pimenov, J. Wu, Q. Xu, C. Cao, J. Chen, W. Xu, L. Kang, and P. Wu, Opt. Express **18**, 17504 (2010).
[34]D. Wang, Z. Tian, C. Zhang, X. Jia, B. Jin, J. Gu, J. Han, and W. Zhang, J. Opt. **16**, 094013 (2014).
[35]V. Savinov, V. A. Fedotov, S. M. Anlage, P. A. J. de Groot, and N. I. Zheludev, Phys. Rev. Lett. **109**, 243904 (2012).
[36]C. Li, C. Zhang, G. Hu, G. Zhou, S. Jiang, C. Jiang, G. Zhu, B. Jin, L. Kang, W. Xu, J. Chen, and P. Wu, Appl. Phys. Lett. **109**, 022601 (2016).
[37]R. Singh, J. Xiong, A. K. Azad, H. Yang, S. A. Trugman, Q. X. Jia, A. J. Taylor, and H.-T. Chen, Nanophotonics **1**, 117 (2012).
[38]V. Savinov, K. Delfanazari, V. A. Fedotov, and N. I. Zheludev, Appl. Phys. Lett. **108**, 101107 (2016).
[39]V. Savinov, A. Tsiatmas, A. R. Buckingham, V. A. Fedotov, P. A. J. de Groot, and N. I. Zheludev, Sci. Rep. **2**, 450 (2012).
[40]R. Singh and N. I. Zheludev, Nat. Photonics **8**, 679 (2014).
[41]N. Laman and D. Grischkowsky, Appl. Phys. Lett. **93**, 051105 (2008).
[42]R. Singh, Z. Tian, J. Han, C. Rockstuhl, J. Gu, and W. Zhang, Appl. Phys. Lett. **96**, 071114 (2010).
[43]M. A. Khazan, "Time-domain terahertz spectroscopy and its application to the study of high-Tc superconductor thin films," Ph.D. thesis (University Hamburg, 2002).
[44]M. C. Ricci and S. M. Anlage, Appl. Phys. Lett. **88**, 264102 (2006).
[45]M. Tinkham, *Introduction to Superconductivity*, 2nd ed. (McGraw-Hill, New York, 1996).
[46]K. K. Mei and G.-C. Liang, IEEE Trans. Microwave Theory Tech. **39**(9), 1545 (1991).
[47]A. Nahata, A. S. Weling, and T. F. Heinz, Appl. Phys. Lett. **69**, 2321 (1996).
[48]Y. Yang, I. I. Kravchenko, D. P. Briggs, and J. Valentine, Nat. Commun. **5**, 5753 (2014).
[49]R. Singh, A. K. Azad, J. F. O'Hara, A. J. Taylor, and W. Zhang, Opt. Lett. **33**, 1506 (2008).